Available online at www.sciencedirect.com
SCIENCE DIRECT®
Microporous and Mesoporous Materials 76 (2004) 233–246
MICROPOROUS AND MESOPOROUS MATERIALS
www.elsevier.com/locate/micromeso

Modeling the occupancy dependence of diffusivities in zeolites

R. Krishna *, D. Paschek, R. Baur

Van 't Hoff Institute for Molecular Sciences, University of Amsterdam, Nieuwe Achtergracht 166, 1018 WV Amsterdam, The Netherlands

Received 6 April 2004; received in revised form 15 August 2004; accepted 16 August 2004

Abstract

The Maxwell–Stefan (M–S), or corrected, diffusivity, in zeolites shows a variety of dependencies on the molecular loading or occupancies. This loading dependence is caused by a variety of factors, including zeolite topology, connectivity, and molecule–molecule interactions, that lead to a decrease or increase in the energy barrier for diffusion. Using the quasi-chemical theory of Reed and Ehrlich [Surf. Sci. 105 (1981) 603–628] for surface diffusion on a square lattice as a basis, a simple model is developed to describe the loading dependence of the M–S diffusivity for a lattice topology with an arbitrary coordination number. The developed model is validated by kinetic Monte Carlo simulations in square, cubic and MFI zeolite topologies. Published Molecular Dynamics simulations of the loading dependence of M–S and self-diffusivities in a variety of zeolite topologies can be modeled using this approach. The M–S formulation allows accurate prediction of the transport and self-diffusivities in binary mixtures using only pure component diffusion data. For the prediction of mixture diffusion, correlation effects also need to be properly quantified and a scheme is suggested for estimation of these effects using data on M–S and self diffusivities of single components.
© 2004 Elsevier Inc. All rights reserved.

Keywords: Maxwell–Stefan theory; Self-diffusion; Monte Carlo simulations; Loading dependence; Molecular dynamics

1. Introduction

The proper description of diffusion of molecules within zeolites is an essential step in the development of reaction and separation processes involving zeolite catalysts and adsorbents [1,2] and it is generally accepted that the Maxwell–Stefan (M–S) diffusion formulation provides a convenient and general framework that can be used in practice [3–5]. For single component diffusion of species i, the M–S formulation:

$$\mathbf{N}_i = -\rho\Theta_i Đ_i \frac{1}{RT}\nabla_{T,p}\mu_i \equiv -\rho\Theta_{i,\mathrm{sat}} Đ_i \frac{\theta_i}{RT}\nabla_{T,p}\mu_i \qquad (1)$$

relates the flux $\mathbf{N}_i$ to the chemical potential gradient $\nabla_{T,p}\mu_i$. In Eq. (1), Θ_i is molecular loading expressed say in molecules per unit cell, $\Theta_{i,\mathrm{sat}}$ is the saturation loading, $\theta_i \equiv \Theta_i/\Theta_{i,\mathrm{sat}}$ is the fractional occupancy, ρ is the zeolite framework density expressed as the number of unit cells per m^3, R is the gas constant, T is the temperature, and $Đ_i$ is the M–S, or corrected diffusivity. For solving practical problems involving single component diffusion it is necessary to have information on the variation of the M–S diffusivity $Đ_i$ with the fractional occupancy θ_i. In the literature on zeolite diffusion, two special scenarios have often been assumed for this occupancy dependence [4,5]. In the *weak confinement* scenario the M–S diffusivity is taken to be independent of the occupancy and identified with the zero-loading diffusivity value

$$Đ_i = Đ_i(0) \qquad (2)$$

In the *strong confinement* scenario the M–S diffusivity is a decreasing function of occupancy following:

$$Đ_i = Đ_i(0)(1-\theta_i) \qquad (3)$$

* Corresponding author. Tel.: +31 20 5257007; fax: +31 20 5255604.
E-mail address: r.krishna@uva.nl (R. Krishna).

1387-1811/$ - see front matter © 2004 Elsevier Inc. All rights reserved.
doi:10.1016/j.micromeso.2004.08.014

Nomenclature

a_i	constants defined in Eq. (19), dimensionless
$D_{i,\text{self}}$	self-diffusivity, $m^2 s^{-1}$
$Đ_i$	Maxwell–Stefan diffusivity of species i in zeolite, m^2/s
$Đ_{ii}$	self-exchange diffusivity, m^2/s
$Đ_{ij}$	binary exchange diffusivity, m^2/s
E	activation energy for diffusion, J/mol
f	parameter defined by Eq. (6), dimensionless
N_i	molecular flux of species i, molecules $m^{-2} s^{-1}$
p	jump probability, dimensionless
r	position coordinate, m
R	gas constant, 8.314 J $mol^{-1} K^{-1}$
t	time, s
T	absolute temperature, K
z	coordination number of lattice, dimensionless

Greek letters

β	parameter defined by Eq. (6), dimensionless
ε	parameter defined by Eq. (6), dimensionless
ν	jump frequency, s^{-1}
θ_i	fractional occupancy of component i, dimensionless
Θ_i	molecular loading, molecules per unit cell
$\Theta_{i,\text{sat}}$	saturation loading, molecules per unit cell
λ	jump distance on lattice, m
$[\Lambda]$	matrix of Onsager coefficients, $m^2 s^{-1}$
μ_i	molar chemical potential, J mol^{-1}
ρ	zeolite density, number of unit cells per m^3

Subscripts

1	component 2 in binary mixture
2	component 2 in binary mixture
i	component i
sat	referring to saturation conditions
i,j	components in mixture

Recently, Skoulidas and Sholl [6,7] have performed molecular dynamics (MD) simulations for a variety of molecules in four different zeolite topologies (MFI, ISV, ITE, and MTW) and demonstrated a rich variety of occupancy dependencies for $Đ_i$ that conform to neither of the two scenarios sketched above. As illustration, consider diffusion of CH_4, CF_4, Ar, SF_6, Ne and Xe in MFI at 298 K; the occupancy dependencies are shown in Fig. 1a. While CF_4 can be considered to follow the strong confinement scenario as an approximation, the weak confinement scenario is not strictly realized for any of the other molecules. For Xe, we note that $Đ_i$ exhibits a slight maximum. SF_6 exhibits a curious inflection behaviour in the loading dependence of $Đ_i$. Intermolecular "interactions", leading to varying degrees of reduction in the energy barrier for diffusion are the root cause of the variety of occupancy dependencies [8–11]. As support for this contention let us consider diffusion of CH_4 in MFI, for which the M–S diffusivity exhbits a slight decrease with increased occupancy; see Fig. 1a. Skoulidas and Sholl [12] have reported MD simulation data on the M–S diffusivity $Đ_i$ for 200, 298, 373 and 473 K at various loadings Θ. From their data we have calculated the activation energy for diffusion as a func-

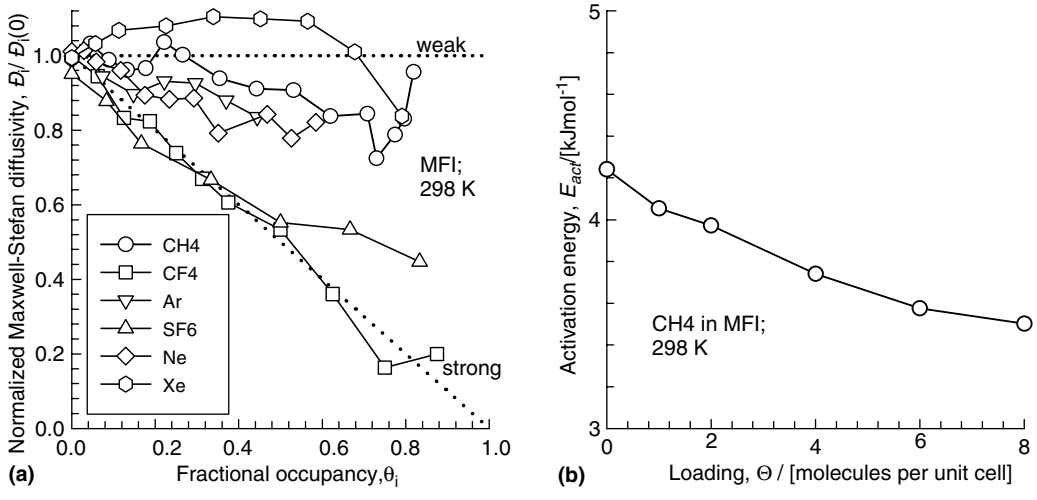

Fig. 1. (a) Occupancy dependences for diffusion of CH_4, CF_4, Ar, SF_6, Ne and Xe in MFI at 298 K. The data are from MD simulations of Skoulidas and Sholl [6,7]. The zero-loading diffusivities and saturation capacities are specified in Table 1. (b) Variation of activation energy of diffusion with loading for diffusion of CH_4 in MFI. The data has been calculated from the MD simulations of Skoulidas and Sholl [12].

tion of the loading Θ; see Fig. 1b. We note a small, yet steady, decrease in the activation energy with increased loading. There is also some experimental evidence to show that the activation energy for diffusion decreases with increased loading; witness the data for diffusion of *n*-butane in MFI as reported in Fig. 4 of Gardner et al. [13].

Clearly, an important factor in describing the occupancy dependence of $Đ_i$ is the quantification of the reduction in the energy barrier for diffusion with increased θ_i. One candidate theory is the quasi-chemical approach of Reed and Ehrlich [14] for describing the diffusion of interacting *atoms* on a square lattice of binding sites, each capable of holding one atom. Adsorbed atoms, or adatoms, on this rigid lattice interact with each other through nearest neighbours only. For each additional atom placed at any of the four nearest neighbour sites surrounded an adatom, the energy of the system is *increased* by δE. To calculate the effective jump rate or diffusivity, we need to know two things: the probability $p^{(j)}$ that an adatom be surrounded by j other adatoms in nearest neighbour positions, as well as the jump rate $v^{(j)}$ of such an adatom. The overall jump rate $v(\theta)$ is then given by

$$v(\theta) = \sum_{j=0}^{z-1} \frac{z-j}{z} p^{(j)} v^{(j)} \tag{4}$$

where z is the coordination number of the lattice ($z = 4$ for a square lattice), giving the number of nearest neighbours,

$$p^{(j)} = \binom{z}{j} \frac{(\varepsilon/f)^j}{(1+\varepsilon/f)^z} = \frac{z!}{j!(z-j)!} \frac{(\varepsilon/f)^j}{(1+\varepsilon/f)^z} \tag{5}$$

and

$$f = \exp\left(\frac{\delta E}{RT}\right); \quad \varepsilon = \frac{(\beta - 1 + 2\theta)f}{2(1-\theta)};$$
$$\beta = \sqrt{1 - 4\theta(1-\theta)(1-1/f)} \tag{6}$$

Assuming a simple model for the jump rate

$$v^{(j)} = v(0) f^j \tag{7}$$

we obtain after substituting Eqs. (5)–(7) in Eq. (4) and application of the polynomial theorem

$$v(\theta) = v(0) \frac{(1+\varepsilon)^{z-1}}{(1+\varepsilon/f)^z} \tag{8}$$

When the zero-loading M–S diffusivity for component i, $Đ_i(0)$ is identified with $\frac{1}{z} v(0) \lambda^2$ where λ is the jump distance on the lattice, we obtain the following relation for the loading dependence of the M–S diffusivity

$$Đ_i(\theta) = Đ_i(0) \frac{(1+\varepsilon)^{z-1}}{(1+\varepsilon/f)^z} \tag{9}$$

In the limiting case where there are no interactions between adatoms, i.e. $\delta E = 0$, we get $f = 1$, $\beta = 1$, $\varepsilon = \theta/(1-\theta)$ leading to the strong confinement scenario described by Eq. (3). We also note that for no combination of the model parameters z and f, does Eq. (9) yield the weak confinement scenario. This is due to the fact that the hopping rates are dependent on the vacancy, and therefore for $\theta = 1$, $Đ_i(\theta) = 0$.

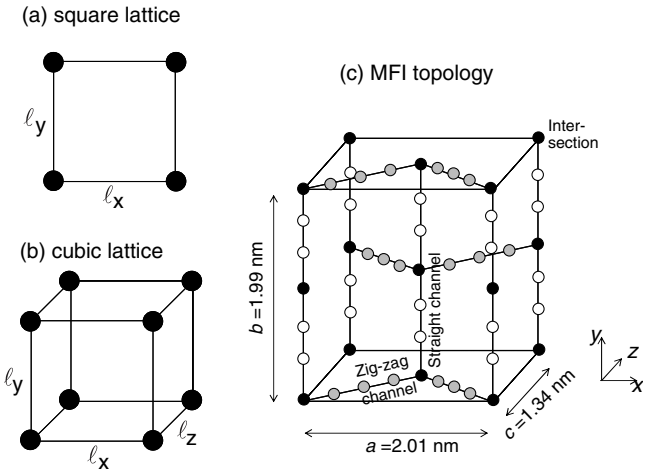

Fig. 2. Unit cells for: (a) square; (b) cubic and (c) MFI lattice topologies. For the square and lattice topologies, the occupation is one molecule per site, indicated by black dots. For simulation of diffusion of methane in MFI, a total of 24 sites are used per unit cell; these sites are indicated as black dots (intersections), white dots (straight channels) and grey dots (zig-zag channels). The distribution of CH_4 molecules per unit cell is as follows: 4 at intersections, 8 within straight channels, and 12 within the zig-zag channels.

Our major objective in this paper is to demonstrate that Eq. (9) affords a convenient and simple approach to describe the occupancy dependence of $Đ_i$ in zeolites. To achieve this objective we perform kinetic Monte Carlo (KMC) simulations in square, cubic and MFI lattice topologies, as depicted in Fig. 2. Once the loading dependence for individual guest–host combination can be quantified, this information can be used to describe the mixture behaviour without additional parameter inputs.

2. KMC simulation methodology

We perform kinetic Monte Carlo (KMC) simulations of a system of adsorbed particles on discrete lattice sites with nearest neighbour interactions. Particles can move from one site to a neighbouring site via hops. The probability per unit time to move from one site to another is determined by a certain hopping rate v. Mixtures of particles are identified by their individual particle mobility. In order to investigate the influence of lattice topology (dimensionality and connectivity) on the diffusivity we have investigated square, cubic and MFI lattice (containing 24 sorption sites) topologies as shown in Fig. 2.

We employ a standard KMC methodology to propagate the system [15–20]. A hop is made every KMC step

and the system clock is updated with variable time steps. For a given configuration of random walkers on the lattice a process list containing all possible M moves to vacant intersection sites is created. Each possible move i is associated with a jump probability ν_i Note that the values depend on the particular type a particle belongs to, as well as on the possible occupation of neighbouring sites. The *mean* elapsed time τ is the inverse of the total rate coefficient

$$\tau^{-1} = \nu_{\text{total}} = \sum_{i=1}^{M} \nu_i \tag{10}$$

which is then determined as the sum over all processes contained in the process list. The actual KMC time step Δt for a given configuration is randomly chosen from a Poisson distribution

$$\Delta t = -\ln(u)/\nu_{\text{total}} \tag{11}$$

where $u \in [0,1]$ is a uniform random deviate. The time step Δt is independent from the chosen hopping process. To select the actual jump, we define process probabilities according to $p_i = \sum_{j=1}^{i} \nu_j/\nu_{\text{total}}$. The ith process is chosen, when $p_{i-1} < \upsilon < p_i$, where $\upsilon \in [0,1]$ is another uniform random deviate. After having performed a hop, the process list is updated. In order to avoid wall effects we employ periodic boundary conditions. We have investigated the finite size effect on the diffusivity and found systems of 10×10 and $6 \times 6 \times 6$ unit cells to be sufficiently large for the 2D and 3D lattices. In order to provide sufficiently accurate data a total of 10^8–10^9 simulation steps were required. These simulations extended to several CPU days on a single IBM SP2 node.

In order to account for nearest neighbour interactions, the transition rates have to be altered if another particle occupies an adjacent site. The employed procedure is illustrated in Fig. 3. It is based on the assumption

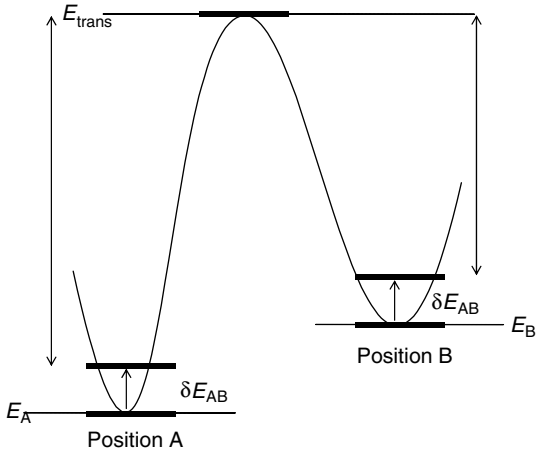

Fig. 3. Energy scheme used for KMC simulations used here. Two particles adsorbed at adjacent sites experience a repulsive interaction energy $\delta E_{\alpha\beta}$.

that the logarithm of the hopping rate is proportional to the relative height of the energy barrier, as for example given by $E_{\text{trans}} - E_A$ for the move from A to B. Consider two neighboring particles at positions A and B. In order to ensure energy conservation, both particles have to experience the same repulsive interaction δE_{AB}. The depth of the potential well of a particle at position A is modified by δE_A which is determined by summing over all possible nearest-neighbor interactions

$$\delta E_A = \sum_B \delta E_{AB} \tag{12}$$

Here B indicates all *occupied* nearest neighbour positions with respect to A. In the KMC scheme the rates of all possible moves of the particle located at A have to be changed by a factor

$$\nu'_{A\to B'} = \nu_{A\to B'} \exp\left(\frac{\delta E_A}{RT}\right) \tag{13}$$

Here B' denotes all empty nearest neighbour positions with respect to A. Since we do not wish to introduce an explicit value for the temperature T here, the Arrhenius term in Eq. (13) is replaced by a product of pair–pair interaction factors f_{AB}

$$\nu'_{A\to B'} = \nu_{A\to B'} \prod_B f_{AB} \tag{14}$$

with

$$f_{AB} = f = \exp\left(\frac{\delta E_{AB}}{RT}\right) \tag{15}$$

Since only nearest neighbour interactions are involved, the scheme is simple and the computational effort is moderate. In our KMC simulations we study the influence of the pair–pair interaction factors f set equal to 1 (no repulsions), 0.5 (attraction), or 1.5, 2 and 2.5 (varying degrees of repulsion).

From the KMC simulations we calculate the M–S diffusivity $Đ_i$ from the mean square displacement of the centre of gravity of all n adsorbed particles:

$$Đ_i = \frac{1}{6}\lim_{\Delta t\to\infty}\frac{1}{\Delta t}\left\langle\left(\frac{1}{n}\sum_{i=1}^{n}(\mathbf{r}_i(t+\Delta t)-\mathbf{r}_i(t))\right)^2\right\rangle \tag{16}$$

These diffusivities correspond to "corrected" diffusivities, as shown in the work of Reed and Ehrlich [21] and Tarasenko et al. [10].

The *self diffusivities* $D_{i,\text{self}}$ are obtained from the mean square displacement of the individual particles:

$$D_{i,\text{self}} = \frac{1}{6}\lim_{\Delta t\to\infty}\frac{1}{\Delta t}\frac{1}{n}\sum_{i=1}^{n}\left\langle(\mathbf{r}_i(t+\Delta t)-\mathbf{r}_i(t))^2\right\rangle \tag{17}$$

The choice of Δt has been discussed in previous publications [17–20].

3. KMC simulation results

The KMC simulations of the M–S diffusivity $Đ_i$ for square and cubic lattices are shown by open symbols in Fig. 4a and b for varying values of the factor $f = 0.5$, 1 and 2. Also shown with continuous solid lines in Fig. 4a and b are the corresponding calculations using the Reed–Ehrlich model, Eq. (9), taking $z = 4$ and 6, respectively, for the square and cubic lattices. The agreement between the KMC simulations and the Reed–Ehrlich model is near perfect as expected, because the KMC simulations were set up using exactly the same physical model underlying the Reed–Ehrlich development. With $f = 1$, $Đ_i(\theta_i)$ follows the strong confinement scenario, described by Eq. (3), as is typical of KMC simulations in which no molecule-molecule interactions are accounted for [17]. The strong influence of the coordination number, z, reflecting the number of nearest neighbours is evident by comparing the results for square and cubic lattices for an occupancy of say $\theta = 0.56$. The normalized M–S diffusivity $Đ_i(\theta)/Đ_i(0) = 1.65$ and 3.44, respectively for the square and cubic lattices, reflecting the strong influence of the *number* of nearest neighbours.

Let us now consider the KMC simulations for diffusion of CH_4 in MFI at 300 K. The jump frequency along the straight channels is taken as $v_{str} = 4.2 \times 10^{11}\ s^{-1}$; for transport along the zig-zag channels we take $v_{zz} = 3.6 \times 10^{11}\,s^{-1}$. These jump frequency values are chosen so as to match the self-diffusivity data of Goodbody et al. [22] in x, y and z directions, as described in our earlier KMC simulation work [18]. The number of sorption sites within the MFI lattice is taken to be 24 per unit cell; these sorption sites are distributed uniformly as indicated by the circles in Fig. 2c. We employ a slight modification with respect to the model proposed in ref. [18] in that the jump rate of molecules in the intersection sites are considered equal to the jump rates of molecules located within the channels. Simulations have been carried out taking the pair interaction factors $f = 1, 1.5, 2$ and 2.5. The results for the normalized M–S diffusivity are presented as open symbols in Fig. 4c. Each of 20 CH_4 molecules located *within* the straight or zig-zag channels "sees" only two neighbours. On the other hand each of the four CH_4 molecule located at the intersections, sees four neighbouring molecules. The weighted-average coordination number for CH_4 diffusion in the MFI topology is $(20 \times 2 + 4 \times 4)/24 = 2.33$. The continuous solid lines in Fig. 4c represent calculations using Eq. (9), taking $z = 2.1$, a "best fit" value for the coordination number. The reason for the deviation from the calculated value of 2.33 is that the jump frequency along the zig-zag channels are lower than that

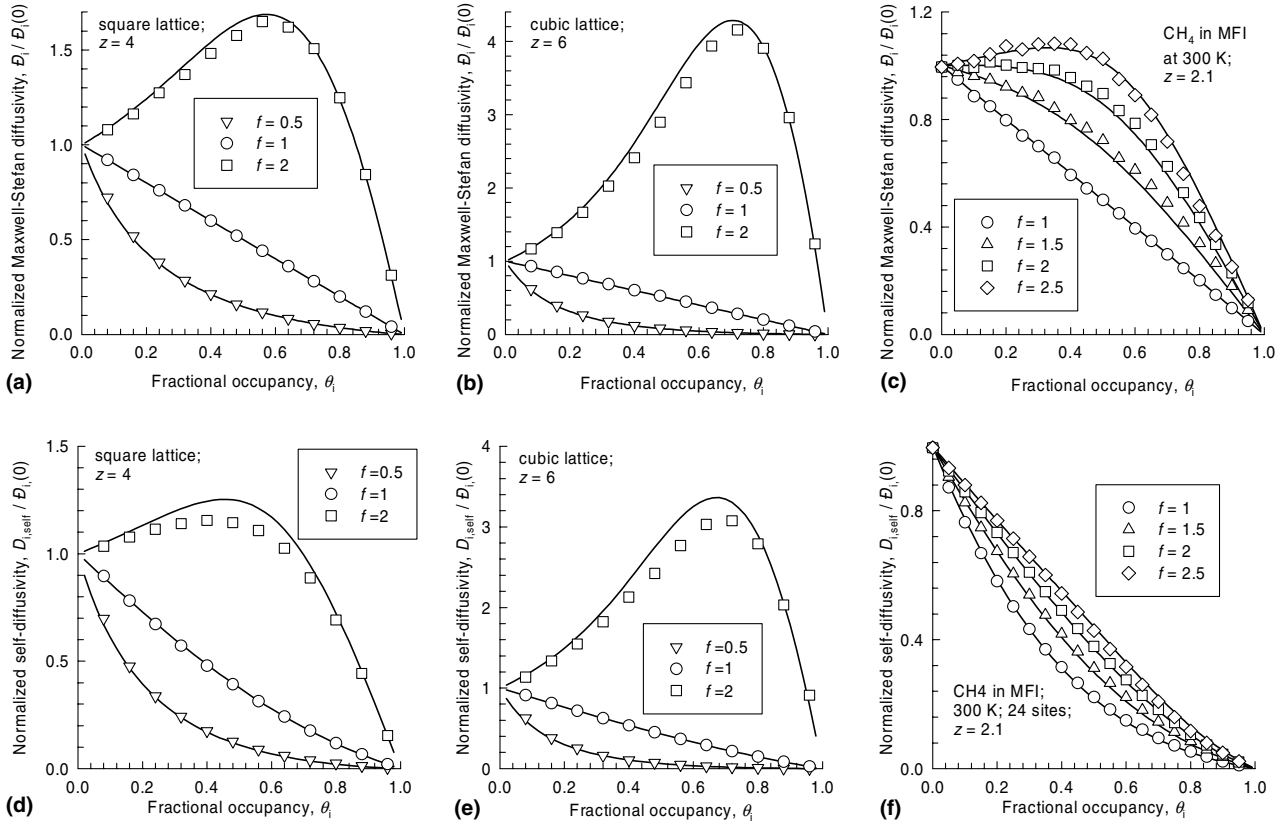

Fig. 4. KMC simulations (open symbols) of normalized M–S diffusivity and self-diffusivity in: (a), (d) square; (b), (e) cubic and (c), (f) MFI lattice topologies. Also shown in (a)–(c) using continuous solid lines are the calculations of $Đ_i$ with the Reed–Ehrlich model, Eq. (9). The self-diffusivity calculated using Eq. (18) are shown using continuous solid lines in (d)–(f).

along the straight channels, resulting in a slightly lower connectivity in practice. In the KMC study of Coppens et al. [23] for the MFI topology, using a lattice with six sites, a coordination number of 2.67 was obtained. If the molecules can be located only at the intersections of MFI, as is the case, for example, with 2-methylhexane [17], we would expect a coordination number of 4.

KMC simulations of the *self*-diffusivities in the (a) square, (b) cubic, and (c) MFI topologies are shown by the open symbols in Fig. 4d–f. The continuous solid lines in Fig. 4d–f were obtained from calculations using the following formula for self-diffusion

$$D_{i,\mathrm{self}} = \frac{1}{\dfrac{1}{Đ_i} + \dfrac{\theta_i}{Đ_{ii}}} \tag{18}$$

where $Đ_{ii}$ is the *self-exchange* coefficient that arises naturally in the M–S formulation for tracer diffusion of a labelled species in an environment of unlabelled species [5]. The parameter $Đ_{ii}/Đ_i$ can be taken as a measure of correlation effects. The lower the value of $Đ_{ii}/Đ_i$, the stronger the influence of correlations. A very large value of $Đ_{ii}/Đ_i$ signifies weak correlations between molecular jumps. The $Đ_{ii}/Đ_i$ is also occupancy dependent and this dependence can be generally described by

$$\frac{Đ_{ii}}{Đ_i} = a_1 \exp(-a_2\theta_i) + a_3 \exp(-a_4\theta_i) \tag{19}$$

following the work of Skoulidas et al. [5]. For the KMC simulations only the first member on the right-hand side of Eq. (19) is required and the parameters a_1 and a_2 were chosen for the three topologies as (a) 2.5, 1, (b) 5, 1 and (c) 0.7, 1.2 based on the information given in Table 2 of Skoulidas et al. [5]. The good agreement between Eq. (18) and the KMC simulations for a variety of values of the interaction parameter for all three topologies implies that the self-exchange coefficient is *not* influenced by the chosen value for f. This is a useful simplification to the description of diffusion in mixtures, in which $Đ_{ii}$ plays a crucial role [5].

4. MD simulated occupancy dependencies in various topologies

We now apply the Reed–Ehrlich model to describe the observed loading dependence of MD simulated diffusivities $Đ_i$ reported by Skoulidas and Sholl [6,7] and Chempath et al. [24] for various molecules in five different zeolite topologies (MFI, ISV, ITE, MTW and FAU). In Fig. 5a and b the MD simulated $Đ_i$ values (open symbols) in MFI are compared with the calculations following Eq. (9), shown with continuous solid lines, in which the interaction parameter f is chosen to "fit" the MD data on $Đ_i$. The zero-loading diffusivities and saturation capacities are as specified in Table 1. Based on the KMC simulation results for CH_4 in MFI, we choose $z = 2.1$ as the coordination number. For CF_4, $Đ_i$ appears to follow the strong confinement behaviour and a choice of $f = 1$ is able to describe this scenario approximately. A more thorough analysis unravels an inflection in the loading dependence [25] at $\Theta = 12$. For both Ar and Ne, a value of $f = 1.7$ is successful in reproducing the MD simulated results. For CH_4, SF_6 and Xe it is necessary to take the interaction parameter f to be occupancy dependent: $f = a_5 \exp(a_6\theta)$, where the chosen values of a_5 and a_6 are specified in Table 1. It is interesting to note that both the maximum for Xe and the inflection behaviour of SF_6 are captured by the Reed–Ehrlich model. In practice the value of f can be estimated from the $E_{\mathrm{act}} - \Theta$ information as presented in Fig. 1b.

Zeolite ISV (ITQ-7) has an intersecting channel structure and the MD simulated loading dependence of $Đ_i$ for CH_4, CF_4, Ar and SF_6 show similar trends as for MFI; see Fig. 5c. The continuous solid lines in Fig. 5c represent the calculations using the Reed–Ehrlich model, Eq. (9) in which we take $z = 2.1$, assuming the same connectivity as for MFI.

The topology of ITE (ITQ-3) consists of cages interconnected to one another through narrow windows. The loading dependence of $Đ_i$ of CH_4, Ar and Ne all show a pronounced maximum (see Fig. 5d), suggesting a substantial decrease in the energy barrier for diffusion with increased loading and this is captured in the Reed–Ehrlich model by a larger f value than for the MFI and ISV topologies. For 3D inter-connected cage structures we should expect the same connectivity as for a cubic lattice and therefore we take $z = 6$.

Zeolite MTW (ZSM-12) consists of 1D channels and the MD simulations of $Đ_i$ show a sharp reduction with increased loading; see the open symbols in Fig. 5e. For the 1D topology of MTW each molecule has two neighbours and therefore we take $z = 2$ in the Reed–Ehrlich model, along with the parameters specified in Table 1. Eq. (9) is capable of portraying the strong reduction in $Đ_i$ with increased loading.

Fig. 5f shows the MD simulation results of Chempath et al. [24] for $Đ_i$ of *n*-alkanes of 1, 2, 3 and 4 carbon atoms in FAU. FAU consists of a 3D network of cages interconnected to one another by large windows; therefore we take the coordination number $z = 6$. For all the linear alkanes of 1, 2, 3 and 4 C atoms the loading dependence of $Đ_i$ corresponds to the strong confinement scenario. The Reed–Ehrlich model with $f = 1$ captures these loading dependencies.

Skoulidas and Sholl [6,7] and Chempath et al. [24] have also reported data on the self-diffusivities $D_{i,\mathrm{self}}$ for the various molecules in the five zeolite topologies. Using Eq. (18) we back calculated the values of $Đ_{ii}/Đ_i$

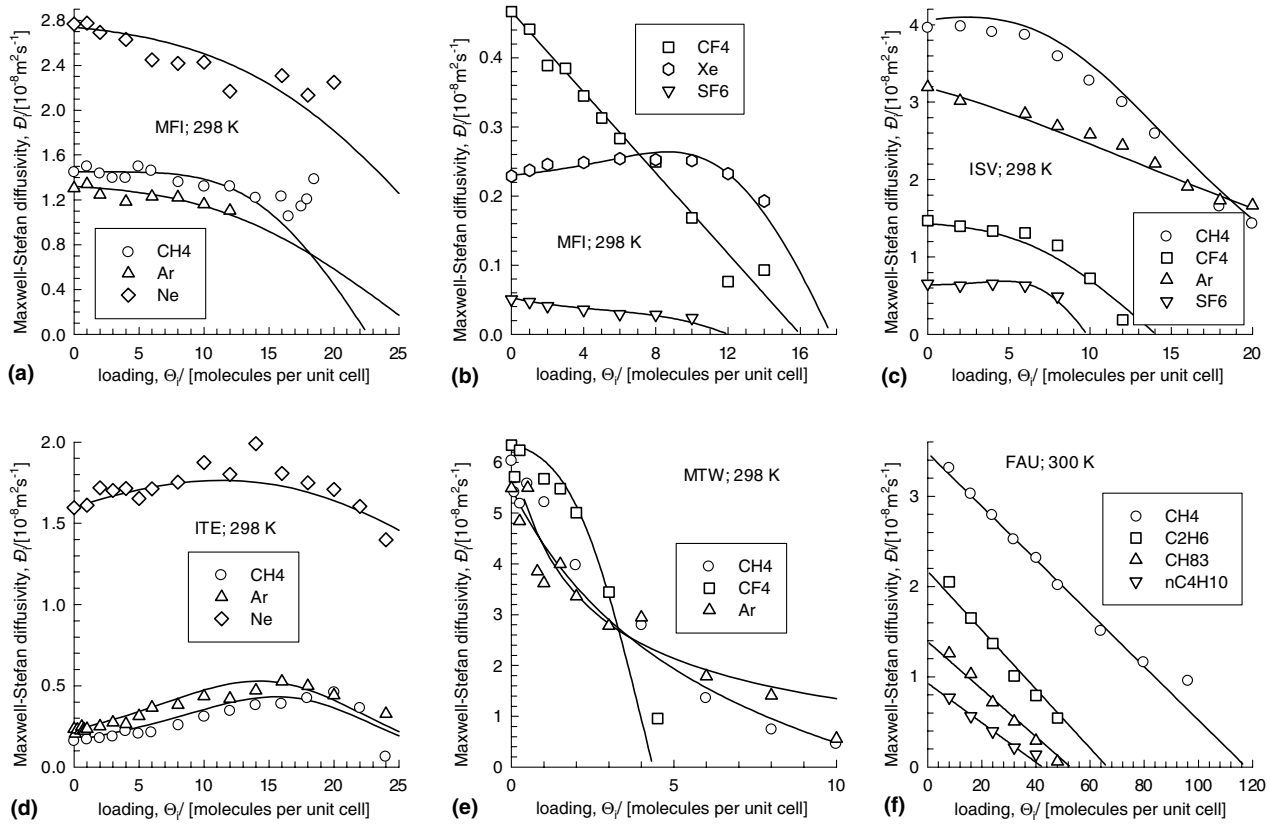

Fig. 5. Loading dependencies for M–S diffusivity $Đ_i$ of various molecules in: (a), (b) MFI; (c) ISV; (d) ITE, (e) MTW and (f) FAU. The open symbols represent data from MD simulations of Skoulidas and Sholl [6,7] and Chempath et al. [24]. The continuous solid lines are from calculations using Eqs. (6) and (9), respectively, with the parameter values as specified in Table 1.

values and these are shown by open symbols in Fig. 6a and b for a few typical molecule-zeolite combinations. Fig. 6a shows the $Đ_{ii}/Đ_i$ values for various molecules in MFI at 298 K. We note that $Đ_{ii}/Đ_i$ decreases with increasing loading, suggesting that correlation effects become stronger at higher loadings. This is to be expected because with increasing loading the chance of finding vacant sites is reduced and many jumps are unsuccessful with the result a molecule will necessarily have to return to its original position [26]. We also note that the higher the saturation capacity, the smaller the value of $Đ_{ii}/Đ_i$. Put another way, the larger the number of adsorption sites in the zeolite, the stronger are the correlation effects.

In Fig. 6b the $Đ_{ii}/Đ_i$ values for CH_4 are shown for five different zeolite topologies: MFI, ISV, ITE, MTW and FAU. The hierarchy of $Đ_{ii}/Đ_i$ is mainly dictated by the connectivity, i.e. the coordination number, z. FAU consisting of cage structures with large windows offers the highest connectivity and highest $Đ_{ii}/Đ_i$. For ITE, which consists of cages connected with narrow windows, $Đ_{ii}/Đ_i$ decreases very sharply with increased occupancy. The poorest connectivity, and consequently the smallest $Đ_{ii}/Đ_i$ is offered by the 1D channel structure of MTW. Interestingly, $Đ_{ii}/Đ_i$ for MTW increases with increased occupancy. For intersecting channel structures of MFI and ISV the $Đ_{ii}/Đ_i$ values lie between those for cages (FAU, ITE) and 1D channels (MTW). The continuous lines in Fig. 6a and b represent "fits" of the MD simulated $Đ_{ii}/Đ_i$ with the empirical model given by Eq. (19), with the constants a_1, a_2, a_3 and a_4 as reported in Table 1.

Now that both loading dependences of $Đ_i$ and $Đ_{ii}/Đ_i$ have been quantified, the self-diffusivity $D_{i,\mathrm{self}}$ can be calculated using Eq. (18). These calculations, shown by the continuous solid lines in Fig. 7a–f for various molecules in the five zeolite topologies. The agreement with the MD simulations is excellent in all the cases.

5. Prediction of diffusivities in mixtures

For n-component diffusion, the M–S equations can be written [4,5,24]

$$-\rho\frac{\theta_i}{RT}\nabla\mu_i = \sum_{\substack{j=1\\ j\neq i}}^{n}\frac{\Theta_j\mathbf{N}_i - \Theta_i\mathbf{N}_j}{\Theta_{i,\mathrm{sat}}\Theta_{j,\mathrm{sat}}Đ_{ij}} + \frac{\mathbf{N}_i}{\Theta_{i,\mathrm{sat}}Đ_i};\quad i=1,2,\ldots,n \tag{20}$$

Table 1
Zero-loading diffusivities, saturation capacities, interaction parameters and self-exchange coefficients for various molecules in various zeolite topologies

Zeolite	Component		Diffusion data					Reed–Ehrlich parameters		
			$Đ_i(0)$	$Đ_{ii}/Đ_i = a_1\exp(-a_2\theta) + a_3\exp(-a_4\theta)$				z	$f = a_5\exp(-a_6\theta)$	
		$\Theta_{i,\mathrm{sat}}$		a_1	a_2	a_3	a_4		a_5	a_6
MFI; 298 K	CH_4	22.6	1.5	0.5	1.45			2.1	1.9	−0.3
	CF_4	16.0	0.467	0.736	1.36			2.1	1.0	0.0
	Ar	26.95	1.32	0.5	2.0			2.1	1.7	0.0
	Ne	34.2	2.74	0.4	−0.5			2.1	1.7	0.0
	Xe	17.7	0.23	0.6	1.2			2.1	2.3	−0.5
	SF_6	12.0	0.053	0.95	1.2			2.1	0.8	−1.0
ISV; 298 K	CH_4	53.5	4.06	0.024	−5.7	0.19	7.3	2.1	3.0	5.0
	CF_4	14.06	1.43	0.592	1.3			2.1	1.7	0.0
	Ar	56.06	3.19	0.028	−5.0	0.19	5	2.1	1.0	1.0
	SF_6	9.81	0.64	1.3	2.0			2.1	1.9	−0.7
ITE; 298 K	CH_4	56.3	0.166	2.0	6.0			6	8.0	4.0
	Ar	44.2	0.23	1.0	1.5			6	4.0	2.0
	Ne	129.1	1.6	0.25	−2.5			6	2.0	3.0
MTW; 298 K	CH_4	39.35	6.24	0.127	−4.01	−0.124	−3.06	2	0.1	1.0
	CF_4	4.36	6.36	0.738	−0.0923	−0.737	−0.0789	2	1.8	0.0
	Ar	12.45	5.49	0.03	60	0.025	−3.5	2	0.5	−0.2
FAU; 300 K	CH_4	117.6	3.48	0.57	0.5			6	1.0	0.0
	CF_4	54.4	1.36	1.0	3	0.12	−2	6	1.0	0.0
	C_2H_6	66.4	2.17	0.78	0.0			6	1.0	0.0
	C_3H_8	52.8	1.39	3.0	5.0	0.12	−3	6	1.0	0.0
	nC_4H_{10}	42.4	0.93	1.8	0.5			6	1.0	0.0

The data in this table is extracted from the MD and GCMC simulations of Skoulidas and coworkers [5–7] and Chempath et al. [24]. The data for Xe in MFI corresponds to that obtained with the force field of Pickett [34]. The saturation capacity $\Theta_{I,\mathrm{sat}}$ has the units of molecules per unit cell. The zero-loading M–S diffusivities $Đ_i(0)$ have the units of $10^{-8}\,\mathrm{m^2\,s^{-1}}$. The other parameters a_1, a_2, a_3, a_4, a_5 and a_6 are dimensionless.

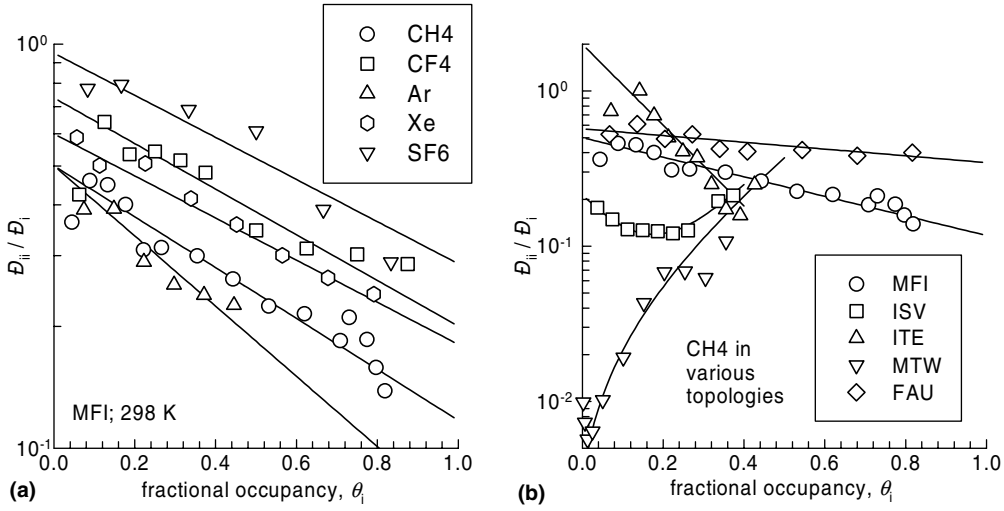

Fig. 6. (a) Variation of $Đ_{ii}/Đ_i$ with loading of: (a) various molecules in MFI at 298 K and (b) CH_4 in MFI, ISV, ITE, MTW and FAU at 298 K. The continuous solid lines represent calculations using Eq. (19) with the parameter values as specified in Table 1.

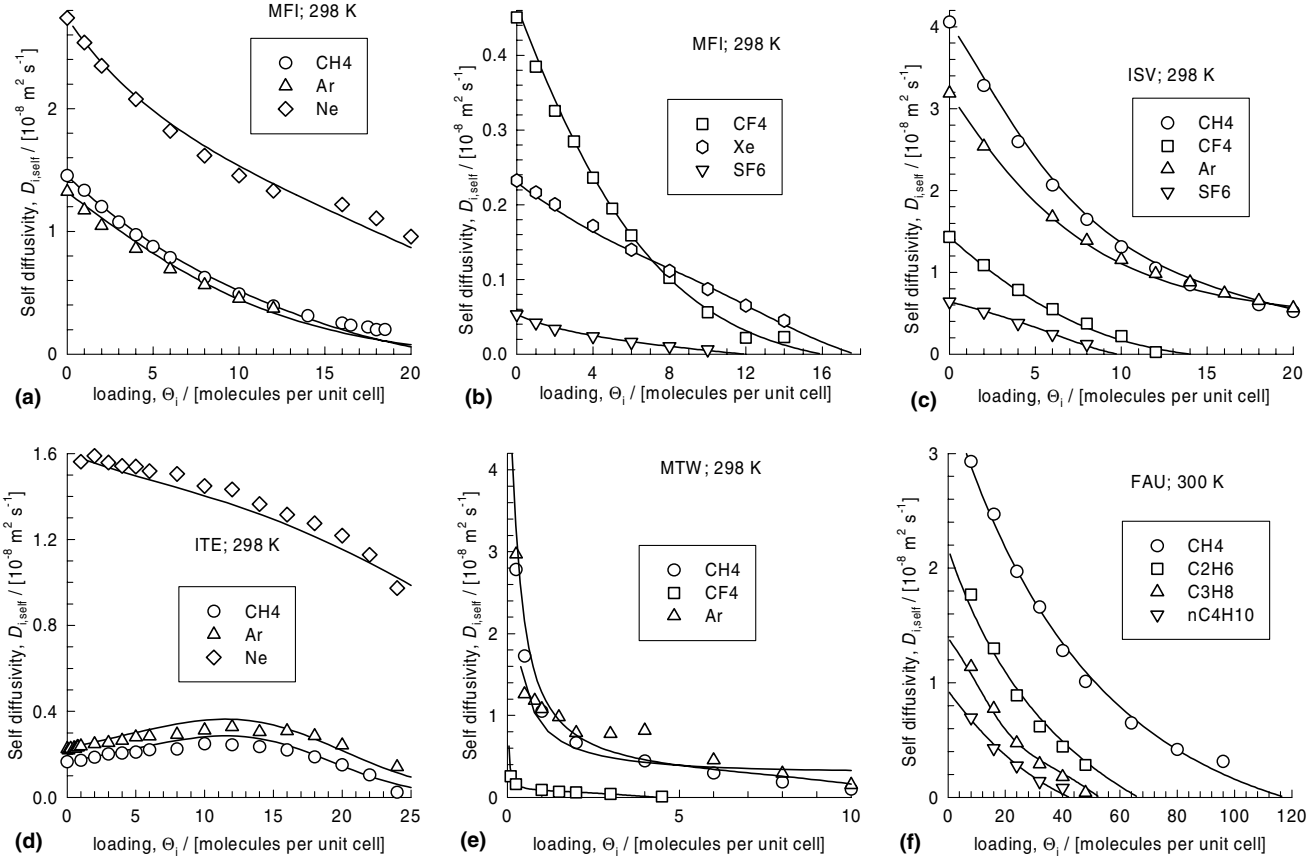

Fig. 7. Loading dependencies for self-diffusivity $Đ_{i,\mathrm{self}}$ of various molecules in: (a), (b) MFI; (c) ISV; (d) ITE; (e) MTW and (f) FAU. The open symbols represent data from MD simulations of Skoulidas and Sholl [6,7] and Chempath et al. [24]. The continuous solid lines are from calculations using Eqs. (6), (9), (18) and (19), with the parameter values as specified in Table 1.

The important advantage of the M–S formulation is that the M–S diffusivities $Đ_i$ in the *mixture* can be estimated from the Reed–Ehrlich development provided we identify θ in Eq. (9) with the total fractional occupancy in the mixture

$$\theta_1 + \theta_2 + \cdots \theta_n = \frac{\Theta_1}{\Theta_{1,\mathrm{sat}}} + \frac{\Theta_2}{\Theta_{2,\mathrm{sat}}} + \cdots \frac{\Theta_n}{\Theta_{n,\mathrm{sat}}} \tag{21}$$

Also, the exchange coefficients $Đ_{ij}$, reflecting *i*–*j* correlations, can be estimated from the self-exchange

coefficients $Đ_{ii}$ using the following interpolation scheme developed earlier [5,24]

$$\Theta_{j,\mathrm{sat}}Đ_{ij} = [\Theta_{j,\mathrm{sat}}Đ_{ii}]^{\Theta_i/(\Theta_i+\Theta_j)}[\Theta_{i,\mathrm{sat}}Đ_{jj}]^{\Theta_j/(\Theta_i+\Theta_j)} = \Theta_{i,\mathrm{sat}}Đ_{ji} \quad (22)$$

We shall verify the predictive capability of the M–S formulation to describe the loading dependence of self- and transport diffusivities in binary mixtures by considering several examples below.

From Eq. (20) the following expressions can be derived for the self-diffusivities of the individual components in a binary mixture [5,27]

$$D_{1,\mathrm{self}} = \frac{1}{\frac{1}{Đ_1}+\frac{\theta_1}{Đ_{11}}+\frac{\theta_2}{Đ_{12}}}; \quad D_{2,\mathrm{self}} = \frac{1}{\frac{1}{Đ_2}+\frac{\theta_1}{Đ_{21}}+\frac{\theta_2}{Đ_{22}}} \quad (23)$$

Jost et al. [28] have published MD simulations for the self-diffusivities in mixtures of CH_4 (1) and Xenon (2) in MFI at 300 K for total loadings $\Theta = 4, 8, 12$ and 16 molecules per unit cell; their data are presented as open symbols in Fig. 8. The calculations following Eqs. (23) and (22) with the pure component parameter values specified in Table 1 are shown by the continuous solid lines. The agreement between the calculations and the MD simulations is remarkably good, especially in view of the fact that all the necessary input parameters have been obtained from pure component data from a different and independent source [6,7].

Snurr et al. [29] have also reported self-diffusivities in binary mixtures of CH_4/CF_4 diffusion in FAU at 300 K for (a) various mixture compositions at a constant total loading $\Theta = 16$ molecules per unit cell, and (b) 50–50 mixture at different mixture loadings; see Fig. 9. These MD simulated self-diffusivities are in very good agreement with the calculations following Eqs. (23) and (22)

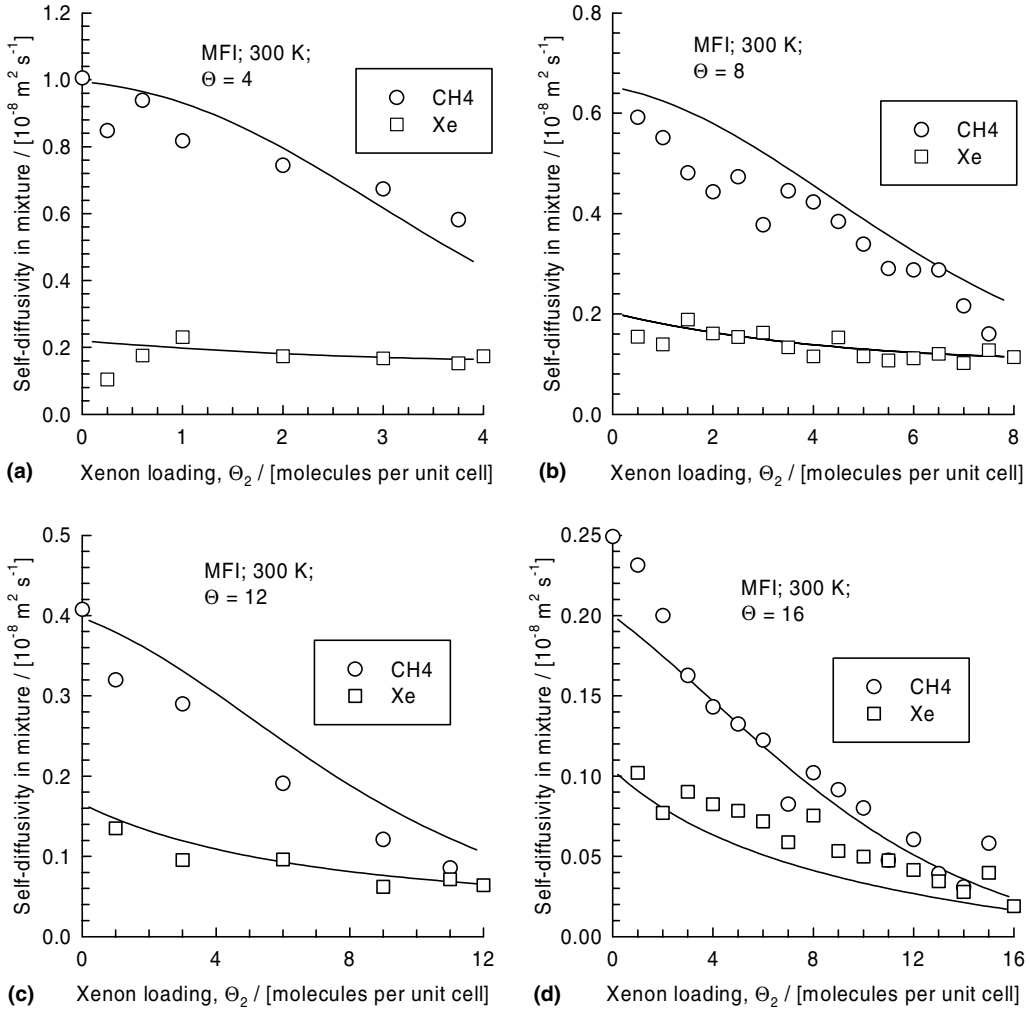

Fig. 8. Comparison of self-diffusivities of CH_4 and Xe in MFI at 300 K from MD simulations of Jost et al. [28] with estimations using Eqs. (22) and (23). The pure component parameter values are specified in Table 1.

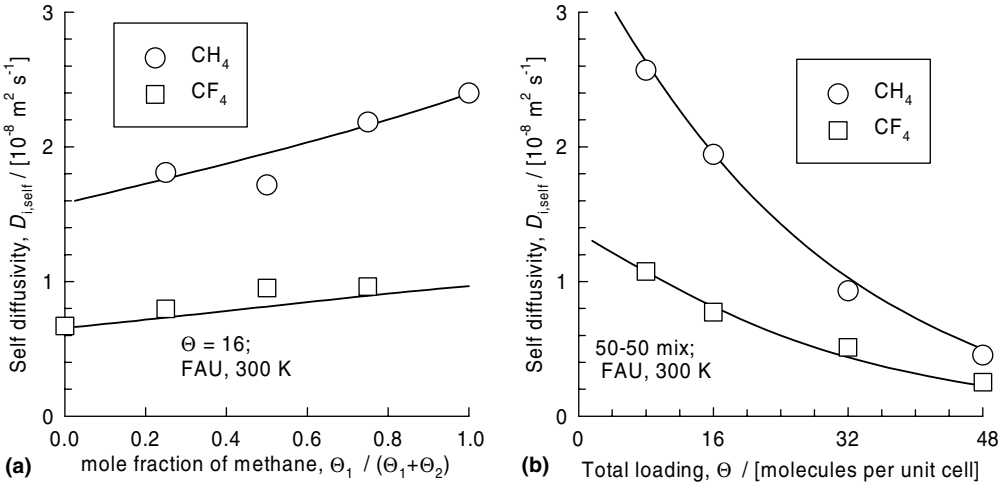

Fig. 9. Comparison of MD simulations (symbols) of Snurr et al. [29] for self-diffusivities in a mixture of CH_4 and CF_4 in FAU at 300 K with estimations (continuous solid lines) using Eqs. (22) and (23). The pure component parameter values are specified in Table 1.

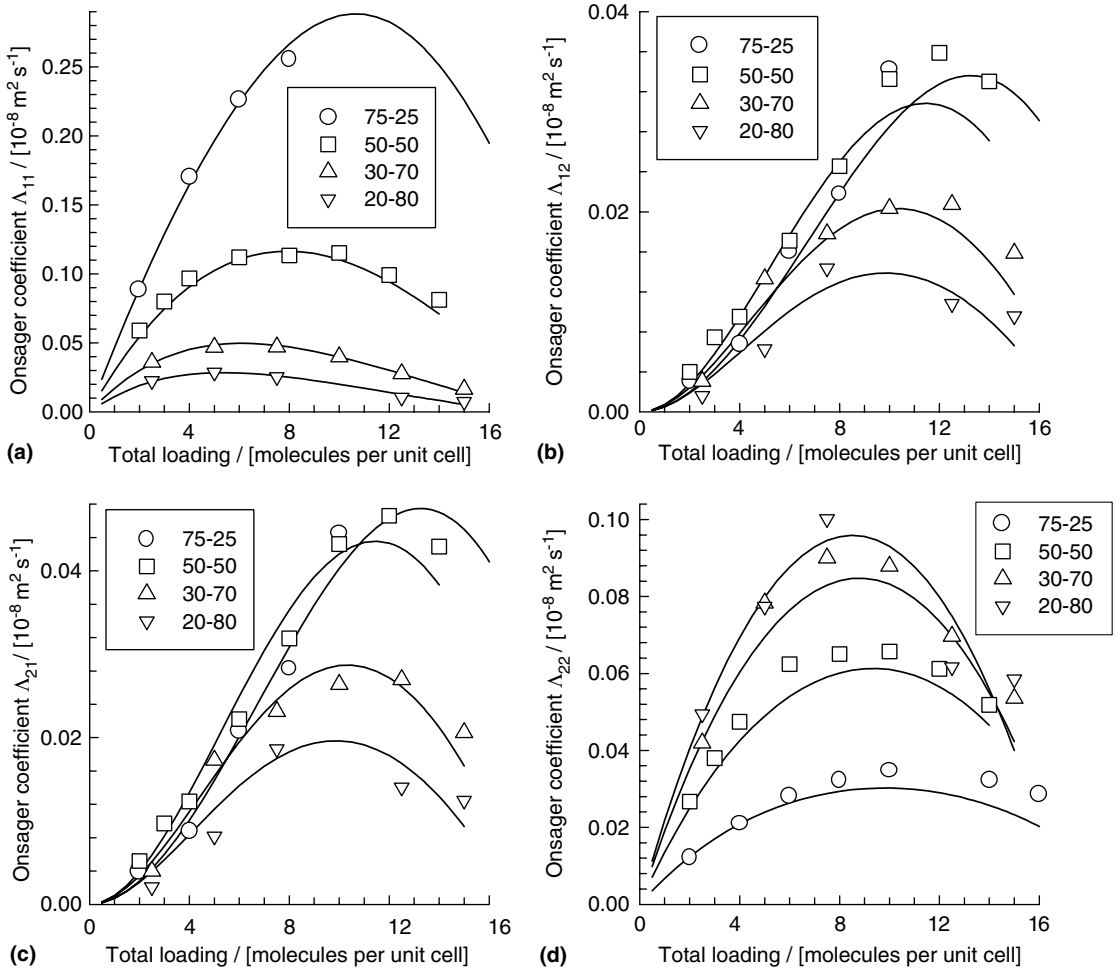

Fig. 10. MD simulations (symbols) of Onsager matrix [Λ] for 75–25, 50–50, 30–70 and 20–80 mixtures of CH_4/CF_4 in MFI at 298 K compared with the calculations using Eqs. (6), (9), (19), (22) and (25). The pure component parameter values are specified in Table 1.

with the pure component parameter values specified in Table 1.

Skoulidas et al. [5] have reported MD simulations of Onsager matrix of diffusivities [Λ], defined by

$$(\mathbf{N}) = -\rho[\Theta_{\text{sat}}][\Lambda]\frac{1}{RT}(\nabla\mu) \tag{24}$$

in binary mixtures of CH_4 and CF_4 in MFI at 298 K; these simulation results are shown by the open symbols in Fig. 10. The elements of $[\Lambda]$ can be related to the M–S diffusivities $Đ_i$ and $Đ_{ij}$ by

$$\begin{bmatrix}\Lambda_{11} & \Lambda_{12}\\ \Lambda_{21} & \Lambda_{22}\end{bmatrix} = \begin{bmatrix}\frac{1}{Đ_1}+\frac{\theta_2}{Đ_{12}} & -\frac{\theta_1}{Đ_{12}}\\ -\frac{\theta_2}{Đ_{21}} & \frac{1}{Đ_2}+\frac{\theta_1}{Đ_{21}}\end{bmatrix}^{-1}\begin{bmatrix}\theta_1 & 0\\ 0 & \theta_2\end{bmatrix} \tag{25}$$

From the pure component data for z, f, and $Đ_{ii}/Đ_i$ for CH_4 and CF_4 as specified in Table 1, along with Eqs. (6), (9), (19), (22) and (25) the elements of $[\Lambda]$ can be estimated; these are shown by the continuous solid lines in Fig. 10. The agreement with the MD simulated values is excellent for the entire range of mixture loadings and mixture compositions. This lends credence to the Reed–Ehrlich model (9) for describing the loading dependence of the M–S diffusivity.

Skoulidas et al. [30] have reported experimental data for the selectivity for permeation of 50–50 mixtures of CH_4 and CF_4 across a MFI membrane at 298 K for different upstream pressures and with pressure drop maintained at 138 kPa; see the open circle symbols in Fig. 11. Numerical integration of the M–S equations (20), taking due account of the loading dependence of the $Đ_i$ and $Đ_{ij}$ allows calculation of the CH_4/CF_4 permeation selectivity (defined here as the ratio of the permeation fluxes); these are shown with the continuous solid lines in Fig. 11. Numerical aspects of the calculation of the membrane permeation fluxes are described by Krishna and Baur [4,31]. In these calculations the pure component isotherm parameters are taken to be the dual site Langmuir parameters as given in Ref. [7]. The mixture loadings are determined using the ideal adsorbed solution theory [32], verified in earlier work for this mixture [5]. The good agreement between the calculations and experimental data is remarkable when we consider that only pure component data (specified in Table 1) is used in these calculations. The correct estimation of the binary exchange coefficient $Đ_{ij}$ using Eq. (22), taking proper account of the loading dependence of the self-exchange coefficients $Đ_{ii}$ using Eq. (19) is a key factor determining mixture permeation selectivity. Correlations tend to slow down the more mobile CH_4 and speed up the more sluggish CF_4, lowering the permeation selectivity when compared to the values on the basis of independent diffusion of the molecules. Such correlation effects are strongly loading dependent as evidenced by the information presented in Fig. 6a. In order to demonstrate the importance of correlation effects we have also performed calculations taking $Đ_{ij}$ to be infinite, leading to negligible correlations; see the continuous dashed lines in Fig. 11. Ignoring correlation effects anticipates a significantly higher permeation selectivity, completely at variance with experimental data.

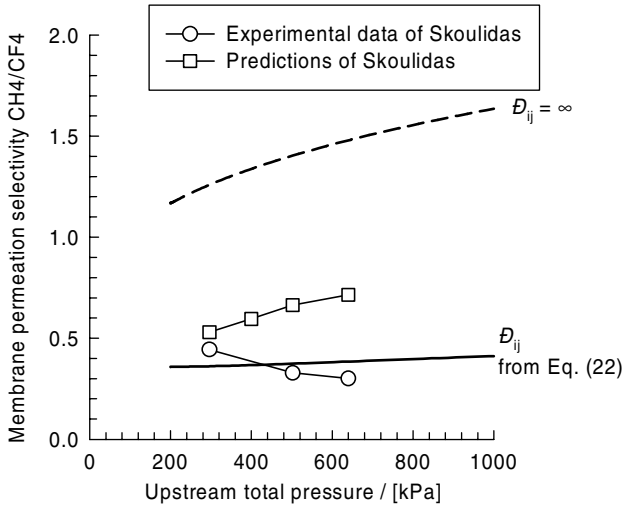

Fig. 11. Selectivity for permeation of 50–50 mixtures of CH_4/CF_4 across an MFI membrane at 298 K as a function of various upstream total pressures. The pressure drop across the membrane is maintained at 138 kPa in all experiments reported by Skoulidas et al. [30]. The experimental data (open circles) are compared with the predictions of the M–S formulation (continuous lines), with two different scenarios for estimation of the binary exchange coefficient $Đ_{ij}$. The numerical details of the membrane permeation calculations are given in refs [4,31]. The predictions of Skoulidas et al. [30] based on *fits* of the binary Onsager matrix obtained from their MD simulations are shown by the open square symbols.

Skoulidas et al. [30] also present their own calculations of the permeation selectivity using fits of (1) the elements of the binary Onsager matrix with 21 constants and (2) fits of the binary adsorption equilibrium using 16 constants; these are shown by the square symbols in Fig. 11. The calculations of Skoulidas et al. [30] are significantly worse than our own predictions using the Reed–Ehrlich model based on only pure component data and far fewer constants. One possible reason the poor predictions of the calculations of Skoulidas et al. [30] is that the loading dependence of correlation effects are not properly described by their fits of mixture transport.

6. Conclusions

The quasi-chemical theory of Reed and Ehrlich [14] describing the occupancy dependence of the M–S diffusivity $Đ_i$, developed for a square lattice with interacting adatoms, has been generalized to a lattice topology with arbitrary coordination number z. Eq. (9) is the key result wherein the factor f quantifies the reduction in the energy barrier for diffusion with increased occupancy. Eq. (9) simplifies to the strong confinement scenario, Eq. (3), for the special case with $f = 1$. KMC simulations

with square, cubic and MFI lattice topologies, with specified values of f, are used to verify Eq. (9). The variety of occupancy dependencies of $Đ_i$ determined by MD simulations [6,7,24] for a variety of molecules in five different zeolite topologies MFI, ISV, ITE, MTW and FAU can be "modeled" by appropriate choice of the interaction factor f and the coordination number z. For describing the variation of the self-diffusivity $D_{i,\mathrm{self}}$ with loading, we need to additionally have information on the magnitude of the correlation effects, quantified by $Đ_{ii}/Đ_i$.

Correlation effects are of essential importance in describing diffusion in mixtures. The M–S formulation provides a method for estimation of self- and transport diffusivities in mixtures from pure component data. This predictive capability has also been demonstrated in this work for various mixtures in MFI and FAU.

The Reed–Ehrlich analytic expression for describing the loading dependence of the M–S diffusivity is particularly convenient for engineering calculations of fluxes of multicomponent mixtures in membranes, adsorbers and catalytic reactors. The crucial Reed–Ehrlich parameter f can be estimated from MD simulations or transition state theory calculations [33].

Acknowledgment

RK, DP and RB acknowledge two grants *Programmasubsidie* and TOP *subsidie* from the Netherlands Foundation for Fundamental Research (CW-NWO) for development of novel concepts in reactive separations.

References

[1] D.M. Ruthven, Principles of Adsorption and Adsorption Processes, John Wiley, New York, 1984.
[2] J. Kärger, D.M. Ruthven, Diffusion in zeolites and other microporous solids, John Wiley, New York, 1992.
[3] F.J. Keil, R. Krishna, M.O. Coppens, Modeling of diffusion in zeolites, Rev. Chem. Eng. 16 (2000) 71–197.
[4] R. Krishna, R. Baur, Modelling issues in zeolite based separation processes, Seperat. Purif. Technol. 33 (2003) 213–254.
[5] A.I. Skoulidas, D.S. Sholl, R. Krishna, Correlation effects in diffusion of CH_4/CF_4 mixtures in MFI zeolite. A study linking MD simulations with the Maxwell–Stefan formulation, Langmuir 19 (2003) 7977–7988.
[6] A.I. Skoulidas, D.S. Sholl, Transport diffusivities of CH_4, CF_4, He, Ne, Ar, Xe, and SF_6 in silicalite from atomistic simulations, J. Phys. Chem. B 106 (2002) 5058–5067.
[7] A.I. Skoulidas, D.S. Sholl, Molecular dynamics simulations of self, corrected, and transport diffusivities of light gases in four silica zeolites to assess influences of pore shape and connectivity, J. Phys. Chem. A 107 (2003) 10132–10141.
[8] S.Y. Bhide, S. Yashonath, Dependence of the self-diffusion coefficient on the sorbate concentration: a two-dimensional lattice gas model with and without confinement, J. Chem. Phys. 111 (1999) 1658–1667.
[9] S.Y. Bhide, S. Yashonath, Types of dependence of self-diffusivity on sorbate concentration in parameter space: a two-dimensional lattice gas study, J. Phys. Chem. B 104 (2000) 2607–2612.
[10] A.A. Tarasenko, L. Jastrabik, C. Uebing, Diffusion of interacting adsorbates on a square lattice, Langmuir 15 (1999) 5883–5892.
[11] F. Nieto, A.A. Tarasenko, C. Uebing, Adsorption and diffusion of repulsively interacting particles on a triangular lattice, Phys. Chem. Chem. Phys. 2 (2000) 3453–3459.
[12] A.I. Skoulidas, D.S. Sholl, Direct tests of the Darken approximation for molecular diffusion in zeolites using equilibrium molecular dynamics, J. Phys. Chem. B 105 (2001) 3151–3154.
[13] T.Q. Gardner, A.I. Flores, R.D. Noble, J.L. Falconer, Transient measurements of adsorption and diffusion in H-ZSM-5 membranes, AIChE J. 48 (2002) 1155–1167.
[14] D.A. Reed, G. Ehrlich, Surface diffusion, atomic jump rates and thermodynamics, Surf. Sci. 102 (1981) 588–609.
[15] S.M. Auerbach, Theory and simulation of jump dynamics, diffusion and phase equilibrium in nanopores, Int. Rev. Phys. Chem. 19 (2000) 155–198.
[16] M.O. Coppens, A.T. Bell, A.K. Chakraborty, Dynamic Monte Carlo and mean-field study of the effect of strong adsorption sites on self-diffusion in zeolites, Chem. Eng. Sci. 54 (1999) 3455–3463.
[17] D. Paschek, R. Krishna, Monte Carlo simulations of self- and transport-diffusivities of 2-methylhexane in silicalite, Phys. Chem. Chem. Phys. 2 (2000) 2389–2394.
[18] D. Paschek, R. Krishna, Diffusion of binary mixtures in zeolites: kinetic Monte Carlo versus molecular dynamics simulations, Langmuir 17 (2001) 247–254.
[19] D. Paschek, R. Krishna, Kinetic Monte Carlo simulations of transport diffusivities of binary mixtures in zeolites, Phys. Chem. Chem. Phys. 3 (2001) 3185–3191.
[20] D. Paschek, R. Krishna, Inter-relation between self- and jump-diffusivities in zeolites, Chem. Phys. Lett. 333 (2001) 278–284.
[21] D.A. Reed, G. Ehrlich, Surface diffusivity and the time correlation of concentration fluctuations, Surf. Sci. 105 (1981) 603–628.
[22] S.J. Goodbody, K. Watanabe, D. MacGowan, J.P.R.B. Walton, N. Quirke, Molecular Simulation of Methane and Butane in Silicalite, J. Chem. Soc. Faraday Trans. 87 (1991) 1951–1958.
[23] M.O. Coppens, A.T. Bell, A.K. Chakraborty, Effect of topology and molecular occupancy on self-diffusion in lattice models of zeolites—Monte Carlo simulations, Chem. Eng. Sci. 53 (1998) 2053–2061.
[24] S. Chempath, R. Krishna, R.Q. Snurr, Nonequilibrium MD simulations of diffusion of binary mixtures containing short *n*-alkanes in faujasite, J. Phys. Chem. B 108 (2004) 13481–13491.
[25] R. Krishna, J.M. van Baten, D. Dubbeldam, On the inflection in the concentration dependence of the Maxwell-Stefan diffusivity of CF_4 in MFI zeolite, J. Phys. Chem. B 108 (2004) 14820–14822.
[26] J. Kärger, S. Vasenkov, S.M. Auerbach, Diffusion in zeolites (Chapter 10), in: S.M. Auerbach, K.A. Carrado, P.K. Dutta (Eds.), Handbook of Zeolite Science and Technology, Marcel Dekker, New York, 2003, pp. 341–422.
[27] R. Krishna, D. Paschek, Self-diffusivities in multicomponent mixtures in zeolites, Phys. Chem. Chem. Phys. 4 (2002) 1891–1898.
[28] S. Jost, N.K. Bar, S. Fritzsche, R. Haberlandt, J. Kärger, Diffusion of a mixture of methane and xenon in silicalite: a molecular dynamics study and pulsed field gradient nuclear magnetic resonance experiments, J. Phys. Chem. B 102 (1998) 6375–6381.
[29] R.Q. Snurr, A. Gupta, M.J. Sanborn, Molecular modeling of multicomponent diffusion in zeolites, in: P.T. Cummings, P.R. Westmoreland, B. Carnahan (Eds.), First International Conference on Foundations of Molecular Modeling and Simulation,

AIChE Symposium Series No. 325, vol. 97, AIChE, New York, pp. 309–312.

[30] A.I. Skoulidas, T.C. Bowen, C.M. Doelling, J.L. Falconer, R.D. Noble, D.S. Sholl, Comparing atomistic simulations and experimental measurements for CH_4/CF_4 mixture permeation through silicalite membranes, J. Membr. Sci. 227 (2003) 123–136.

[31] R. Krishna, R. Baur, Diffusion, adsorption and reaction in zeolites: modelling and numerical issues. Available from <http://ct-cr4.chem.uva.nl/zeolite/>, 2003.

[32] A.L. Myers, J.M. Prausnitz, Thermodynamics of mixed gas adsorption, AIChE J. 11 (1965) 121–130.

[33] C. Tunca, D.M. Ford, A transition-state theory approach to adsorbate dynamics at arbitrary loadings, J. Chem. Phys. 111 (1999) 2751–2760.

[34] S.D. Pickett, A.K. Nowak, J.M. Thomas, B.K. Peterson, J.F.P. Swift, A.K. Cheetham, C.J.J. Denouden, B. Smit, M.F.M. Post, Mobility of adsorbed species in zeolites—a molecular-dynamics simulation of xenon in silicalite, J. Phys. Chem. 94 (1990) 1233–1236.